

Structure and Magnetism in λ -MnO₂. Geometric Frustration in a Defect Spinel

J. E. Greedan,* N. P. Raju, A. S. Wills, C. Morin, and S. M. Shaw

*Brockhouse Institute for Materials Research and Department of Chemistry,
McMaster University, Hamilton, Ontario L8S 4M1, Canada*

J. N. Reimers

Moli Energy Ltd., 20000 Stewart Crescent, Maple Ridge, B.C. V2X 9E7, Canada

Received March 23, 1998. Revised Manuscript Received June 16, 1998

λ -MnO₂, a metastable form of manganese dioxide, retains the cubic spinel structure upon lithium removal from LiMn₂O₄ by soft chemical methods, either electrochemical or acid leaching. The minimum lithium content, achieved by the latter route at pH 1, is Li_{0.10}-MnO₂, which is in reasonable agreement with previous reports. For lithium contents near the minimum value, long-range antiferromagnetic order sets in below $T_N = 32$ K, and Curie–Weiss susceptibility behavior is found above 125 K, with fitting constants, $\theta_c = -104(4)$ K and $C = 1.97(2)$ emu-K/mol. This value of C is consistent with the lithium content found analytically. The susceptibility is remarkably field dependent in the temperature range near T_N for some samples with larger lithium contents, which might be understood in terms of field-induced short-range ferromagnetic correlations. Neutron diffraction studies show a complex magnetic order described by a propagation vector $k = (1/2, 1/2, 1/2)$ (128 Mn moments per magnetic unit cell) and confirm the $T_N = 32$ K. A model for the magnetic structure is proposed that is consistent with the neutron intensities. The complexity of the magnetic structure is consistent with the geometric frustration inherent in the Mn sublattice, which is comprised of a three-dimensional array of corner-sharing tetrahedra. The properties of λ -MnO₂ are compared and contrasted with those of β -MnO₂, with the rutile structure, and the pyrochlore Y₂Mn₂O₇, with the same topology for the Mn(4+) sublattice.

Introduction

The methods of soft chemistry or “chimie douce” allow the synthesis and study of solid materials that are thermodynamically unstable under standard preparation conditions dictated, as they typically are, by solid-state reaction kinetics. The subject of the work described here is λ -MnO₂, one of the metastable forms of manganese dioxide, for which the thermodynamically stable form is β -MnO₂ or pyrolusite with the rutile structure. λ -MnO₂, first reported to result from acid leaching of lithium from the spinel LiMn₂O₄, retains the structure of the parent phase.¹ Further systematic studies confirmed that acid concentrations near pH 1 were most efficient at lithium removal with final products of composition Li_{0.03}MnO₂.² λ -MnO₂ also results from electrochemical removal of Li from LiMn₂O₄ cathodes in solid-state lithium battery cells during standard charge/discharge cycling. Powder X-ray diffraction (PXRD) confirms the retention of the spinel framework, $Fd\bar{3}m$, with $a_0 = 8.029(1)$ Å to be compared with the cell constant of the parent LiMn₂O₄, $a_0 = 8.245(1)$ Å.² The Mn ions occupy the 16d sites in $Fd\bar{3}m$ and thus form a three-dimensional (3D) array of corner-sharing tetrahedra (Figure 1a). This exact magnetic

sublattice is found in pyrochlore structure oxides, which also crystallize in $Fd\bar{3}m$ symmetry. Corner-sharing tetrahedral magnetic lattices satisfy one of the conditions for geometric magnetic frustration, the other being the presence of dominant nearest neighbor antiferromagnetic exchange interactions.^{3,4} Clearly (see Figure 1b) it is not possible to arrange four spins at the corners of a regular tetrahedron in a mutually antiparallel pattern, two spins will always be frustrated.

Geometrically frustrated systems often exhibit unusual magnetic properties that stem from their enormous ground-state spin degeneracies and the concomitant difficulty in selecting a unique ground state.^{4–6} To contrast geometrically frustrated and conventional antiferromagnets, it is useful to review the characteristics of the latter. The thermal evolution of such systems can be discussed conveniently in terms of three regimes; they are, the paramagnetic, the long-range ordered, and the short-range ordered or “critical” regimes.

At the highest temperatures is found the paramagnetic state in which the spin–spin correlations are spatially random and dynamically fluctuating. At the lowest temperatures there is the long-range ordered

(1) Hunter, J. C. *J. Solid State Chem.* **1981**, *39*, 142.
(2) Mosbah, A.; Verbaere, A.; Tournoux, M. *Mater. Res. Bull.* **1983**, *18*, 1375.

(3) Anderson, P. W. *Phys. Rev.* **1956**, *102*, 1008.
(4) Villain, J. Z. *Phys.* **1978**, *B33*, 31.
(5) Reimers, J. N.; Berlinsky, A. J.; Shi, A.-C. *Phys. Rev.* **1991**, *B43*, 865.
(6) Reimers, J. N. *Phys. Rev.* **1992**, *B45*, 7287.

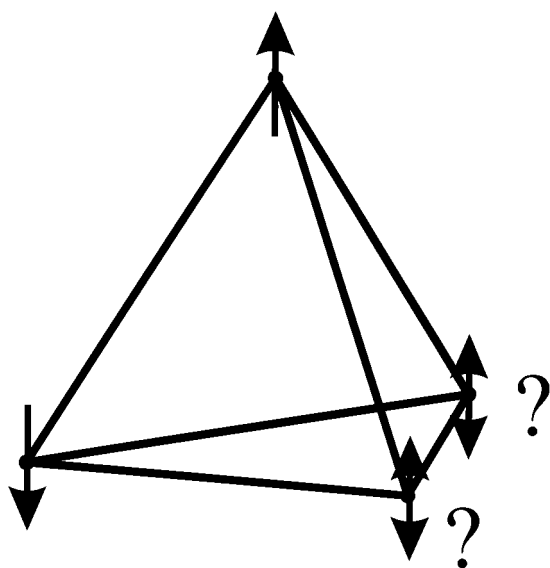
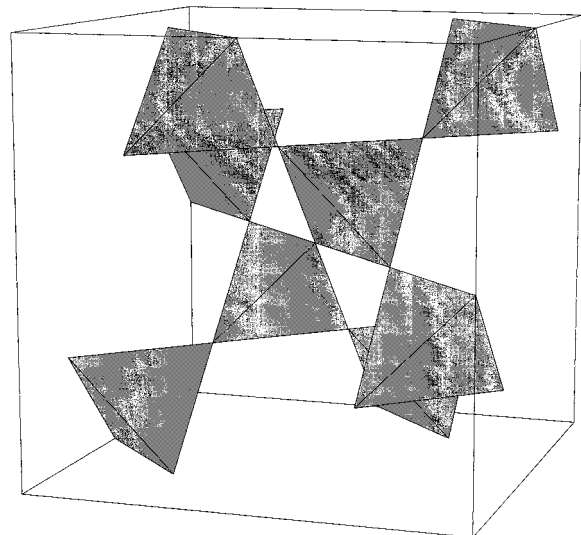


Figure 1. (a) The 3D corner-sharing tetrahedral lattice formed by the 16c and 16d sites in $Fd\bar{3}m$ and found on the B-site of spinels and both cation sites for pyrochlore materials. (b) Illustration of the spin frustration inherent in the regular tetrahedron with dominant nearest neighbor antiferromagnetic exchange.

state in which a unique ground-state spin structure exists, characterized by static order established on an essentially infinite length scale. Usually, the spin structure, called the magnetic structure, is collinear in that for each sublattice of spins pointing in a given direction there exists an equally populated sublattice for which the spin direction is orientated by 180° with respect to the first. Anisotropy forces may act to misalign the sublattices by a few degrees, but the collinear structure remains clearly recognizable. The highest temperature at which an ordered domain of "infinite" length dimension exists is called the "critical" temperature or T_c . For antiferromagnets this is often denoted T_N or the Neel temperature. The transition between the paramagnetic and long-range ordered states is the short-range or "critical" regime in which finite size-ordered domains grow (with decreasing temperature) at the expense of the paramagnetic state. Typically, the critical regime exists over a very narrow temperature interval of a few degrees Kelvin above T_c

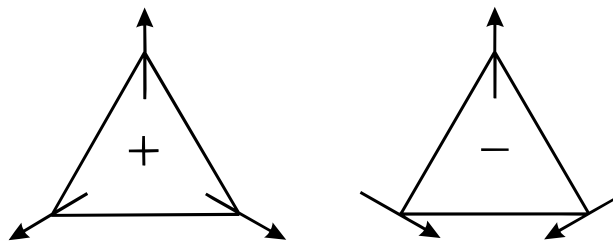


Figure 2. The 120° spin configuration, showing the inherent degeneracy due to chirality.

at the most. Geometrically frustrated systems depart from this typical behavior pattern in two significant ways. First, the thermal existence range for the short-range ordered or critical regime is unusually wide, perhaps several tens of degrees Kelvin. The second, which is even more remarkable, concerns the lowest temperature regime and here two broad classes of materials emerge. In one case, the frustration is reflected in the adoption of a noncollinear ground-state magnetic structure, the most famous being the 120° structure (Figure 2) found in many triangular magnetic lattices. In this case, a finite ground-state degeneracy is retained due to the chiral nature of the spin pattern, as illustrated. In the other case, the system cannot find a unique or even mildly degenerate ground state and a spin glasslike state results, which has also been called "cooperative paramagnetism", in which the spins freeze with respect to dynamics but exhibit no long-range spatial order.⁴ In the first category are found most frustrated triangular antiferromagnets and also most spinel structure oxides.⁷ In the second group one finds several pyrochlore oxides, LiNiO_2 and a few other examples.⁸⁻¹⁰ Of particular relevance to λ - MnO_2 is the pyrochlore $\text{Y}_2\text{Mn}_2\text{O}_7$ in which the same $\text{Mn}(4+)$ ion exists on a sublattice of the same topology. This compound is remarkable, showing no low-temperature long-range order and many physical properties characteristic of spin glasses.¹¹ It is in this context, then, that the magnetic properties of λ - MnO_2 are of interest and an initial investigation has been undertaken.

Experimental Section

Sample Preparation. LiMn_2O_4 . This compound was prepared by solid-state reaction starting with intimately mixed and pelletized Li_2CO_3 and Mn_2O_3 . The reaction was carried out in a stream of flowing oxygen according to a heating schedule in which the pellets were heated to 650°C over 6 h, kept at 650°C for 12 h, and fired at 800°C for an additional 3 h before furnace cooling to room temperature. Phase purity was monitored by the Guinier X-ray method. A black powder was obtained.

λ - MnO_2 . *Acid Leaching.* Samples were prepared by acid treatment of LiMn_2O_4 at room temperature. Reactions were carried out in aqueous HCl at pH 1.0 and 2.0 for 20 h with continuous stirring and pH monitoring. The samples, which

(7) Poole, C. P.; Farach, H. A. *Z. Phys.* **1982**, *B47*, 55.

(8) Greedan, J. E.; Reimers, J. N.; Stager, C. V.; Penny, S. L. *Phys. Rev.* **1991**, *B43*, 5682.

(9) Reimers, J. N.; Dahn, J. R.; Greedan, J. E.; Stager, C. V.; Liu, G.; Davidson, I.; von Sacken, U. J. *Solid State Chem.* **1993**, *102*, 542.

(10) Gaulin, B. D. In *Magnetic Systems with Competing Interactions*; Diep, H. T., Ed.; World Scientific: Singapore, 1994; pp 286–326; Gingras, M. J. P., *ibid.*, pp 238–285; Schiffer, P.; Ramirez, A. P. *Comments Condens. Matter Phys.* **1996**, *18*, 21.

(11) Reimers, J. N.; Greedan, J. E.; Kremer, R. K.; Gmelin, E.; Subramanian, M. A. *Phys. Rev. B* **1991**, *43*, 3387.

changed color from black to dark brown, were recovered by filtration. The filtrate was analyzed for lithium content.

Electrochemical Preparation. λ -MnO₂ was prepared by charging a battery cell based on a LiMn₂O₄ spinel cathode. The cell was constructed as follows. LiMn₂O₄ prepared by standard solid-state methods ($a_0 = 8.2383$ Å) was assembled into a 18650 size (413A⁺) Li ion cell by coating a slurry mix made of active material, binder, carrier solvent, and conducting diluent, onto Al foil. Anodes were made by coating a slurry mix made of graphitized Meso Carbon Micro Beads (MCMB), conductive diluent, carrier solvent, and binder, onto Cu foil. The carrier solvent is baked off during the electrode-coating process. The separator is made of porous polypropylene. The electrolyte was LiPF₆ salt dissolved in a mixture of alkyl-carbonate solvents.

Cells were charged at a constant current of 40 mA, which corresponds to a 30 h rate. When the cell reached 4.3 V, the charging method was switched to constant voltage mode, allowing the current to decay to <5 mA, and the cell to equilibrate. At this state of charge, the graphite anode is at 70 mV versus Li/Li⁺ and the spinel material is therefore at 4.23 V versus Li/Li⁺, which corresponds to a delithiated stoichiometry ($x \approx 0$ in Li_xMn₂O₄).

The spinel material was recovered from the cell by washing the charged cathode electrode with the same carrier solvent used on the coating process. This process redissolves the binder. The resulting slurry was then rinsed with acetone and centrifuged three times. The centrifuge procedure removes a large portion of conductive graphite diluent. The sample was then dried at 90 °C for 6 h and X-rayed. The lattice constant was 8.0429(8) Å and the peak widths were about double those of the precursor material. A graphite (002) reflection was also observed, indicating some of the conductive diluent was still remaining.

Lithium Analysis. Lithium analysis was accomplished using ICP emission spectroscopy with a Jarrell-Ash ICAP-9000 instrument. Approximately 50 mg of the samples were dissolved in warm HCl and then diluted to 1000 mL with distilled, deionized H₂O to give an expected concentration of <10 µg/mL of Li. Standard solutions were prepared from Fisher 1000 µg/mL reference solution in concentrations spanning the expected range.

X-ray Powder Diffraction. The PXRD patterns were obtained using a 100 mm Guinier-Hagg camera with CuK_{α1} radiation and a silicon internal standard. Films were read with a computer-controlled line scanner (LS-20, KEJ Instruments, Täby, Sweden).

Magnetic Measurements. Magnetic data were collected using a SQUID magnetometer (Quantum Design) at a variety of applied fields over the temperature range of 5 to 300 K.

Neutron Diffraction. Data at zero applied field were collected at the McMaster Nuclear Reactor using $\lambda = 1.3920$ Å neutrons over a temperature range from 15 to 300 K. For room-temperature measurements, the samples were contained in a thin-walled vanadium can, whereas for low temperatures, an aluminum can, sealed with an indium wire gasket, and helium exchange gas were used. Temperature was controlled by a closed-cycle refrigerator to ± 0.1 K. Data analysis was performed using DBWS PC9600 and GSAS Rietveld refinement software packages.

The DUALSPEC instrument, C5, at the Chalk River Nuclear Laboratories was used to collect data in magnetic fields up to 1.0 T. The experiments were performed in a magnet cryostat with neutrons of wavelength $\lambda = 2.37044$ Å in double-axis mode.

Results and Discussion

Sample Characterization. Previous work had established that most of the lithium could be removed from LiMn₂O₄ by acid leaching at pH 1, giving samples of composition Li_{0.10}MnO₂¹ or Li_{0.03}MnO₂,² with reported unit cell constants, $a_0 = 8.03$ Å. The three samples of nominal composition MnO₂ studied here, prepared by

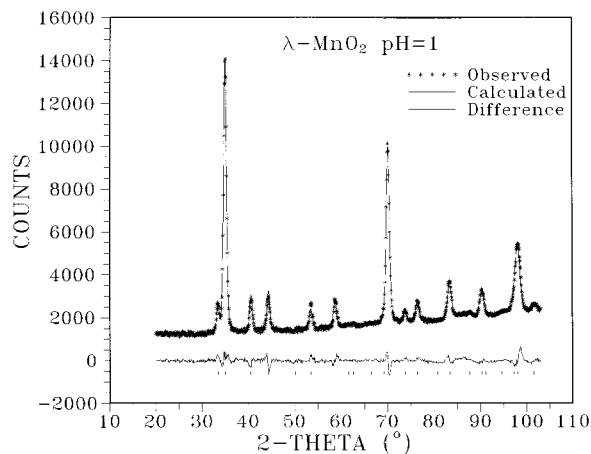


Figure 3. Rietveld refinement of neutron diffraction data for λ -MnO₂, the pH 1 sample, at 295 K.

acid leaching at pH 1 and 2 and by electrochemical deintercalation, gave very similar cell constants to within 0.1% of the literature values and showed only slight variations among themselves. Lithium content analysis of the pH 1 sample gave a composition of Li_{0.10}-MnO₂ in good agreement with the literature¹ and $a_0 = 8.0407(7)$ Å. The cell constants for the electrochemical and pH 2 samples were 8.0429(2) and 8.034(2) Å, respectively. It was not possible to obtain lithium content analyses for the pH 2 and battery samples because of the presence of second phases in each case.

Structure Refinement. Refinement of the structure from neutron powder data for the pH 1 sample (Figure 3 and Table 1) gave a more precise value for the oxygen position parameter, $x = 0.2625$ (1), than that available from earlier PXRD data.² The derived Mn–O distance of 1.9149(8) Å is in the range expected for Mn⁴⁺.

It is not clear from the previous or present work if the spinel form of MnO₂ can be stabilized without finite amounts of Li⁺. To date such a material has not been reported.

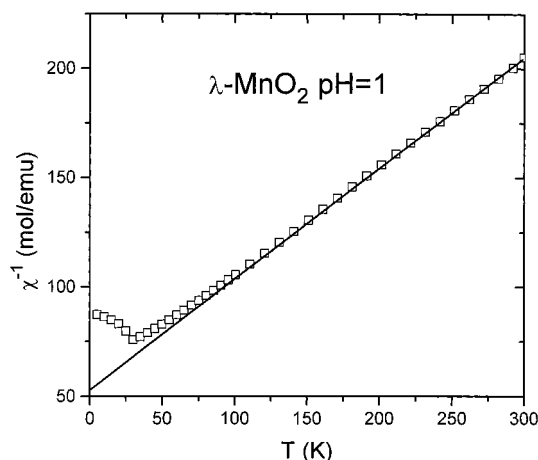
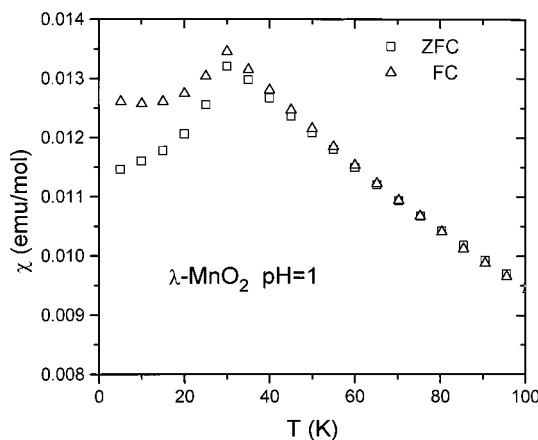
Magnetism. All three samples of λ -MnO₂ studied here show a prominent common feature, namely, a susceptibility maximum in the range 30–32 K (Figures 5–7). There appears to be a slight sample dependence, the pH 1 material giving $T(\chi_{\max}) = 30$ K, whereas for the other two samples, the maximum is near 32 K. In all cases, an antiferromagnetic ordering is indicated.

For the pH 1 sample, the Curie–Weiss law is obeyed above ~ 125 K (Figure 4), with best fit parameters $C = 1.97(2)$ emu-K/mol and $\theta_c = -104(4)$ K. The Curie constant is slightly larger than the spin only value of 1.87 emu-K/mol for Mn⁴⁺ and is consistent with the analytical results that show a lithium content of $\sim 10\%$, which implies an equivalent concentration of Mn³⁺, $S = 2$, $C = 3.00$ emu-K/mol. Detailed fits for the other samples were not undertaken because of the presence of second phases, graphite in the battery sample, and a small impurity in the pH 2 material. Inverse susceptibility plots of both samples showed behavior similar to that for pH 1, except that the deviations from the Curie–Weiss law occur in the opposite sense; that is, χ^{-1} values are smaller than the Curie–Weiss line extrapolation, suggesting the presence of ferromagnetic domains in the short-range ordered regime above the apparent ordering temperature of 32 K.

Table 1. Rietveld Refinement Results for λ -MnO₂ (pH 1, 295 K) Neutron Diffraction ($\lambda = 1.392 \text{ \AA}$)^a

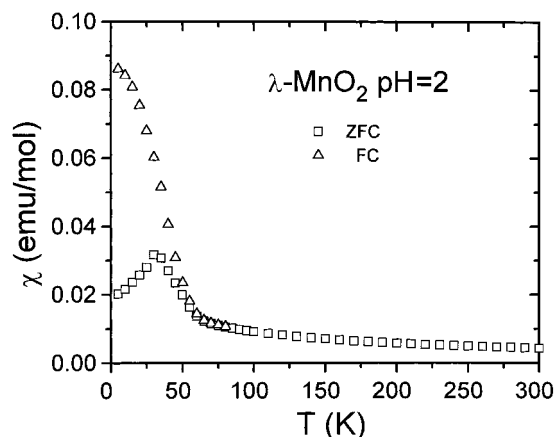
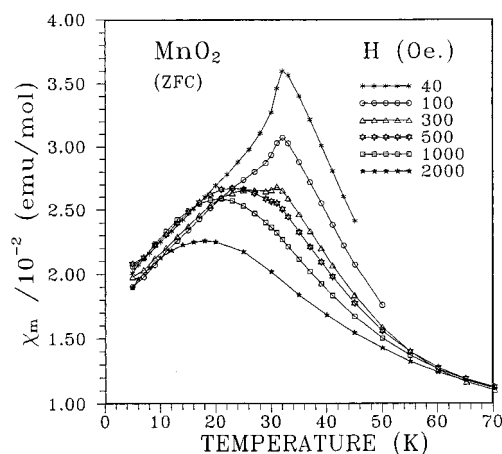
parameter	value	parameter	value
a_0 (Å)	8.0407(7)	space group	$Fd\bar{3}m$ (#227)
2θ range (deg)	20–103	positions:	Mn(16d) 0.5, 0.5, 0.5
step size (deg)	0.10		O(32e) $x = 0.2625(1)$
R_B	0.055	isotropic thermal parameters B (Å ⁻²)	Mn 0.10(7)
R_{wp}	0.046		O 0.80(17)
R_E	0.022	distances (Å)	Mn–O 1.9149(8)
goodness of fit	2.1	angles (deg)	
profile points (N)	831	O–Mn–O	180.0
parameters refined (P)	14		96.17(3)
independent hkl	24	Mn–O–Mn	83.83(3)
			95.85(5)

$$^a R_B = \sum |I_0 - cI_c| / \sum I_0; R_{wp} = [\sum w(y_o - cy)^2 / \sum wy_o^2]^{1/2}; R_E = [N - P / \sum wy_o^2]^{1/2}.$$

**Figure 4.** Inverse magnetic susceptibility for λ -MnO₂, the pH 1 sample. The Curie–Weiss fit is indicated.**Figure 5.** Field-cooled versus zero-field-cooled susceptibility data for the acid leached sample, pH 1. The applied field is 100 Oe.

The θ_c value is negative, consistent with the apparent antiferromagnetic ordering but is not unusually large, giving a ratio $|\theta_c|/T_N = 3$, which does not necessarily imply a strongly frustrated antiferromagnet.¹⁰ One should apply caution in assessing the importance of this ratio criterion, as will be discussed in a later section.

Significant differences between the samples also appear upon examination of the susceptibility data near the transition temperature as a function of sample history; that is, field-cooled (FC) versus zero-field-cooled (ZFC) runs, and the strength of the applied field. The pH 1 sample shows a minimal ZFC–FC variation (Figure 5), with a clear maximum appearing in both curves. By contrast, for pH 2, the maximum disappears

**Figure 6.** Field-cooled versus zero-field-cooled susceptibility data for the acid leached sample, pH 2. The applied field is 100 Oe.**Figure 7.** Zero-field cooled susceptibility data at a variety of applied fields for the electrochemically prepared sample.

in the FC data that approach a saturation at low temperatures, consistent with a ferromagnetic response (Figure 6). The electrochemical sample displays a quite spectacular field dependence (Figure 7), which shows only ZFC data. The maximum that is discernible at very low fields of 40 and 100 Oe is essentially gone by 300 Oe. For higher applied fields, the sharp maximum is replaced by a broad maximum centered near 20 K, the position of which moves to lower temperatures with increasing field. At 5 K, a hysteresis is even seen (Figure 8).

All of the results just presented indicate the presence of a ferromagnetic component in the magnetic microstructure of two of the samples, pH 2 and the electro-

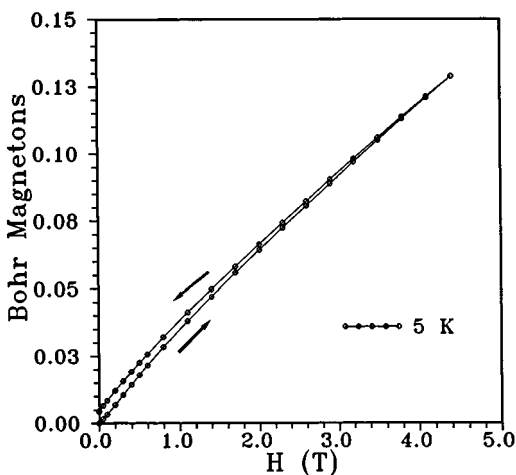


Figure 8. Hysteresis in λ -MnO₂ at 5 K, the electrochemically extracted sample.

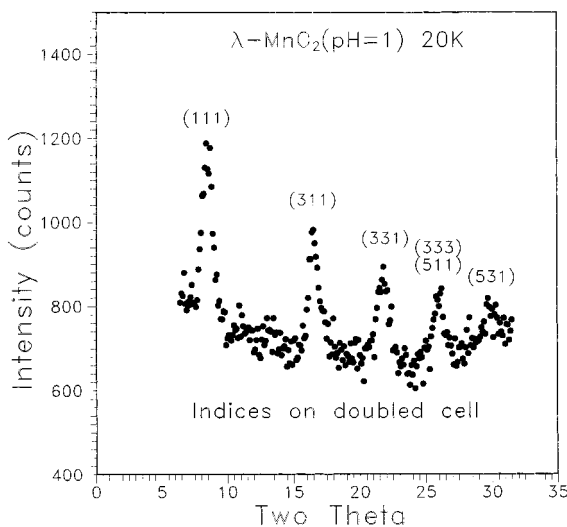
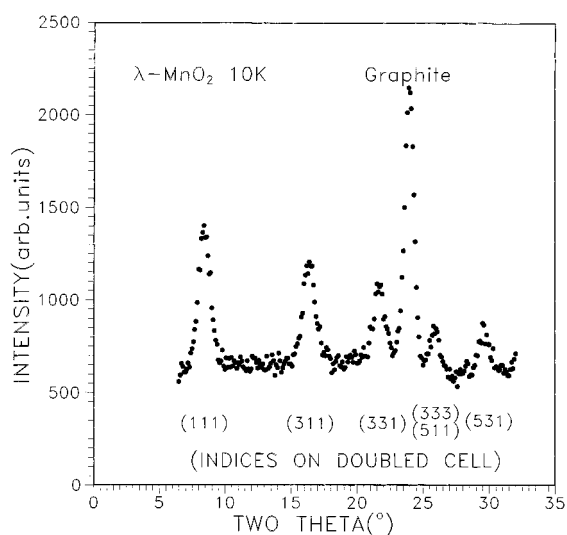


Figure 9. (a) Neutron diffraction pattern of λ -MnO₂, the electrochemical sample, at 12 K in the low-angle region showing the development of magnetic reflections that can be indexed on a doubled cubic cell with the indices as labeled. (b) The corresponding data for the pH 1 sample at 20 K.

chemical, which responds to the applied field thereby masking the underlying antiferromagnetism of λ -MnO₂.

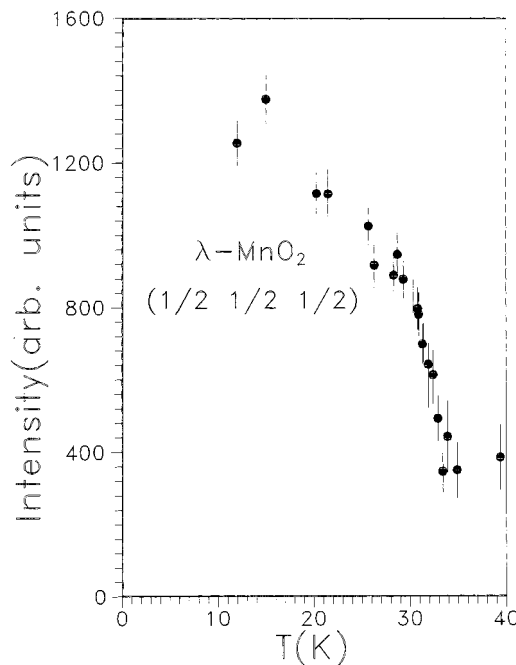


Figure 10. The temperature dependence of the $(\frac{1}{2}\frac{1}{2}\frac{1}{2})$ magnetic reflection intensity for the electrochemical sample.

Magnetic Neutron Diffraction. In neutron diffraction patterns obtained at temperatures well below 30 K, several Bragg peaks appear at positions that require indexing on a doubled chemical cell (Figure 9a). The data are for the battery-derived material, but all three samples showed the same pattern, as illustrated in Figure 9b for the pH 1 sample. These observations strongly support the onset of long-range antiferromagnetic order at low temperature, with an ordering wave vector, $k = (\frac{1}{2}\frac{1}{2}\frac{1}{2})$ and 128 Mn moments per magnetic unit cell.

The thermal variation of the intensity of the superlattice reflections (Figure 10), shows a rapid decrease just above 30 K and confirms the association of these features with magnetic order. That the intensities do not fall to zero is due to the presence of significant short-range order above T_N . One method of locating T_N from such data is to plot the peak width (fwhm) of the magnetic reflections versus temperature as done for the intense $(\frac{1}{2}\frac{1}{2}\frac{1}{2})$ peak in Figure 11. The clear increase above 32.5 K can be used to estimate the ordering temperature. Close examination of the superlattice reflections below and above T_N discloses the surprising fact that the positions of the magnetic reflections show a very strong shift to higher angles in passing through the ordering temperature, as seen in Figure 12 for $T = 25.7$ K and 33.4 K. A more extensive examination (Figure 13), shows clearly the very abrupt shift for $(\frac{1}{2}\frac{1}{2}\frac{1}{2})$ which has an onset temperature of ~ 32.3 K, in excellent agreement with the fwhm and the bulk susceptibility data. It should be emphasized that this shift is enormous. It would correspond to a 6% decrease in the magnetic unit cell constant over a temperature interval of ~ 1 K. For comparison, the overall decrease in the chemical unit cell constant upon cooling from 295 to 10 K is only 0.16%.

From Figure 14, diffuse magnetic scattering is seen up to at least 50 K, which indicates an unusually broad temperature regime for the persistence of short-range

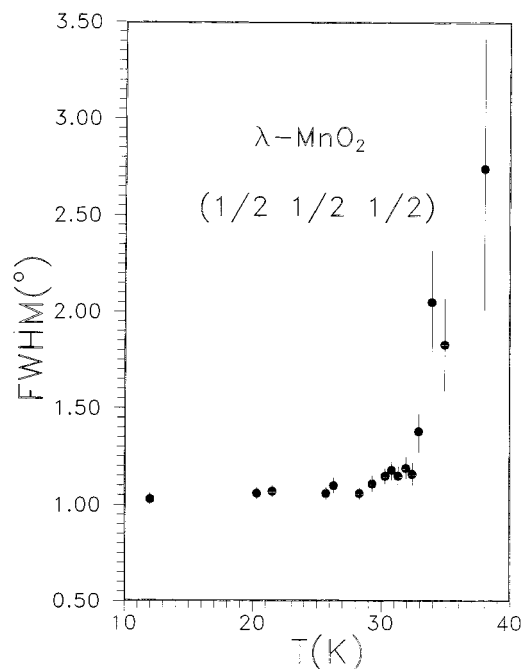


Figure 11. The temperature dependence of the peak width (fwhm) for the $(1/2 1/2 1/2)$ magnetic reflection.

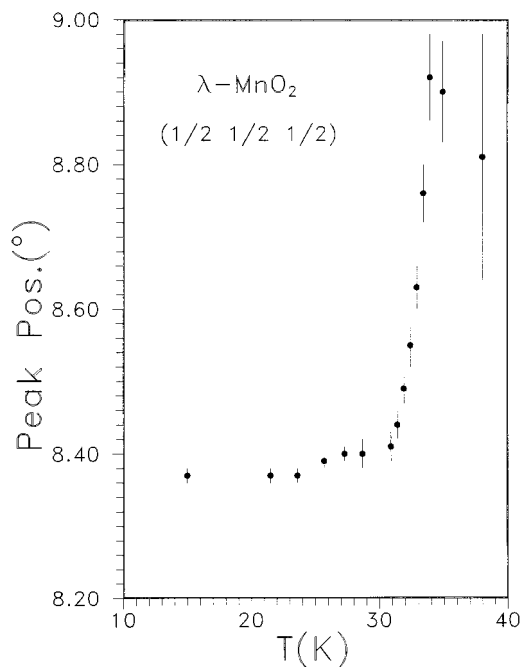


Figure 13. Abrupt shift in the peak position of the $(1/2 1/2 1/2)$ magnetic reflection with temperature.

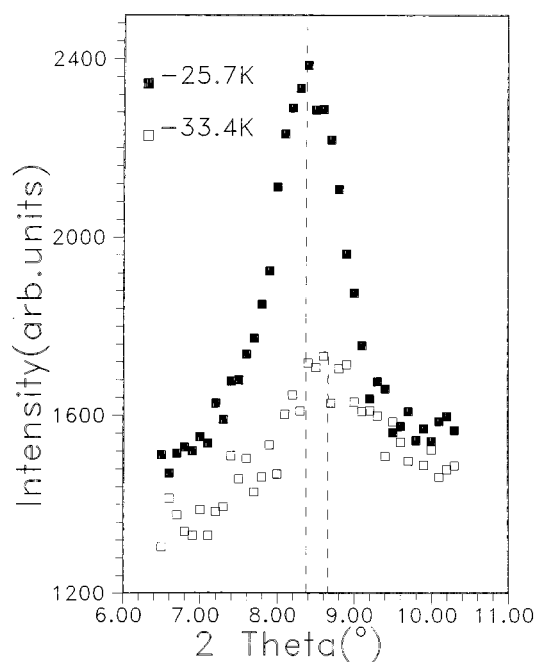


Figure 12. Peak position of the $(1/2 1/2 1/2)$ reflection at two temperatures, 25.7 and 33.4 K.

order. A very rough estimate of the correlation length ξ in the diffuse regime can be obtained from

$$\xi = 1/[\Gamma_{\text{obs}}^2 - \Gamma_{\text{res}}^2]^{1/2}$$

where the Γ_{obs} values are the peak widths expressed in units of $Q = 4\pi \sin \theta / \lambda$ and Γ_{res} is the resolution-limited peak width. Correlation lengths obtained in this way range from ~ 22 Å just above T_N at 33.0 K to 5 Å at 40 K. The observations just described (i.e., the presence of an apparently very complex magnetic ordering with 128 Mn spins per unit cell and an unusually broad short-range ordered thermal regime) are consistent with geometric frustration. Additionally, that the diffuse

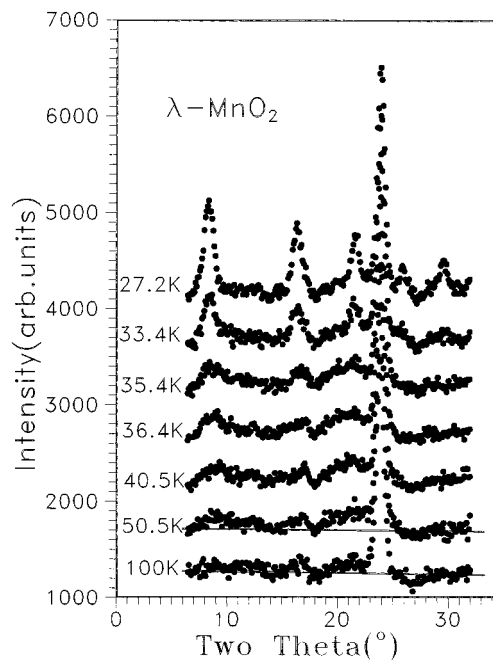


Figure 14. Temperature dependence of the magnetic Bragg peaks just below (27.2 K) and above T_N .

magnetic scattering occurs at positions not commensurate with the magnetic unit cell underscores the level of complexity present in this system.

Given the remarkable field dependence of the bulk susceptibility, neutron diffraction data were collected on the battery-derived sample in applied fields to monitor possible changes to the magnetic structure. The results in Figure 15 indicate essentially no change in the intensities of the magnetic reflections in fields up to 1.0 T. This result reinforces the view that the behavior of the bulk susceptibility arises because of ferromagnetic domains that may be induced by application of a small field. The origin of such domains could be associated with the low levels of Mn^{3+} , which must

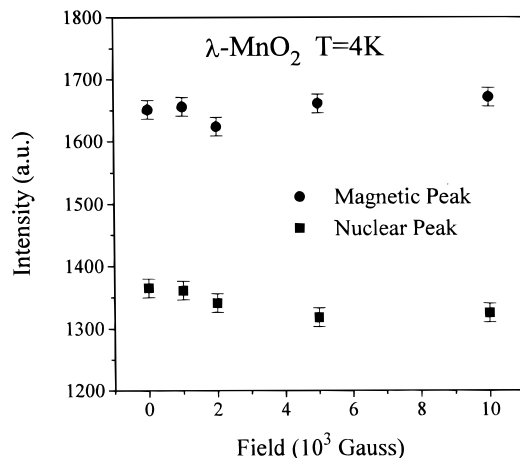


Figure 15. The intensity of the $(1/2, 1/2, 1/2)$ magnetic reflection in fields up to 1.0 T.

be present in all of the samples as a result of the residual lithium content. One could invoke a mechanism, such as double exchange, which plays a dominant role in the ferromagnetism found in the mixed valence $\text{Mn}^{3+}/\text{Mn}^{4+}$ perovskites. On the contrary, such behavior has never been documented for spinel structure materials such as LiMn_2O_4 , where the $\text{Mn}^{3+}/\text{Mn}^{4+}$ ratio is 1:1.¹² It is clear that further study is warranted and, for example, SANS (small-angle neutron scattering) in small fields would be particularly valuable in elucidation of the magnetic microstructure.

Magnetic Structure. Nearly all known spinel structure oxides in which only the B or octahedral site ions are magnetic exhibit long-range antiferromagnetic order but at rather low temperatures.⁷ A variety of magnetic structures have been proposed, most determined from neutron powder diffraction data more than 30 years ago. The observation of all-odd indices for the magnetic reflections is consistent with a face-centered magnetic cell and requires that spins related by the translation $(1/2, 1/2, 1/2)$ must have opposed orientations as pointed out previously.¹³

We examined three possible models for the magnetic structure and these are represented in Figure 16 as the projections onto $(0\ 0\ l)$ of the moments that lie in the planes at $z = 0, 1/8, 1/4,$ and $3/8$. The moments in the second half of the unit cell are reversed. Circles and triangles correspond to different distinct sublattices. Black and white fills relate moments that are antiparallel. The first two structures correspond to four sublattice models and the latter has two sublattices. Models I and II are those proposed previously for GeNi_2O_4 and GeCo_2O_4 , respectively.^{13,14} In model I, each moment is surrounded by two moments of each of the other sublattices, which leads to a structure in which each tetrahedron has one moment from each of the sublattices. In model II, two of these six neighboring spins are parallel and four are antiparallel. This arrangement leads to a magnetic structure in which there are four different types of tetrahedral units made up of both two and four sublattices. In model II, any

given moment is surrounded by two moments of its own type and four that are antiparallel, which leads to a structure in which the tetrahedra contain moments from both sublattice 1 or 2 and can simply be thought of as containing alternating chains of one moment type that are parallel to the $[110]$ and $[1, -1, 0]$ directions. Model II is related to model III by the removal of the degrees of freedom present in the B and $-B$ sublattices. Calculations show that model I is not compatible with the experimental intensities because it fails to predict the presence of the (111) reflection. Those calculated for model III did however compare well. The extra degrees of freedom provided in model II did not improve the fit significantly and model III is thus proposed to describe the magnetic ordering at low temperatures in $\lambda\text{-MnO}_2$.

The magnetic structure was refined in the P1 space group with the constraints $a = b = c$ and $\alpha = \beta = \gamma = 90^\circ$. This unit cell contains 128 Mn atoms. Particular problems were encountered in the analysis of the magnetic diffraction pattern because refinement packages are not yet designed to allow the refinement of such a large number of magnetic atoms. GSAS was used for this work because it did allow all atoms to be entered. However, limits on the number of atoms in any particular constraint prevented free refinement of the orientation of the moment vectors. Instead they were determined by finding the best agreement between calculated and experimentally observed intensities for a number of possible moment orientations. A moment of unit length was defined using the angle from the a -axis (ang-**a**) and the angle from the c -axis (ang-**c**). The projections of the moment along the $a, b,$ and c -axes (proj-**a**, proj-**b**, and proj-**c**, respectively) were calculated. This orientation was used for the Mn chains parallel to the (110) direction (sublattice A) and the antiparallel orientation for the chains parallel to the $(-1, 1, 0)$ directions (sublattice $-A$). Observed magnetic scattering has only significant intensity in the range 7 to 31.5° and the least squares refinement program GENLES was run using only these data. In addition to the magnetic scattering, this reduced data set contains the (002) reflection of graphite. The cycles were carried out with only the histogram scale factor as a refinable variable and the value of χ^2 noted. This procedure was repeated for 5° increments in both ang-**a** and ang-**c** between the limits $0-360^\circ$ and $0-180^\circ$, respectively. Figure 17 displays the χ^2 as a function of both ang-**a** and ang-**c**. The minimum value of χ^2 corresponded to ang-**a** = 180° and ang-**c** = 45° . The absolute scaling required for calculation of the magnitude of the magnetic moment vectors was then manually carried out by comparison of the magnetic reflections with those MnO_2 reflections present in the entire data set and lead to a refined saturated moment on the Mn sites of $2.78(9)\mu_B$. This result is in good agreement with the spin only value of $3\mu_B$. The refined profile pattern for the magnetic refinement is displayed in Figure 18; the final values of χ^2 and R_{wp} are 1.572 and 5.02%, respectively, with 17 variables.

Relevant Comparisons. It is instructive to compare the magnetic properties of $\lambda\text{-MnO}_2$ with both the rutile structure material, $\beta\text{-MnO}_2$ and the pyrochlore $\text{Y}_2\text{M}_2\text{O}_7$, which presents the same ion, Mn^{4+} , on a sublattice of identical topology. Relevant features of all three materials are collected in Table 2.

(12) Shimakawa, Y.; Numata, T.; Tabuchi, J. *J. Solid State Chem.* **1997**, *131*, 138.

(13) Bertaut, E. F.; Qui, VuVan; Pauthenet, R.; Murasik, A. *J. Phys.* **1964**, *25*, 516.

(14) Plumier, R. *C. R. Acad. Sci. Paris* **1967**, *264*, 278.

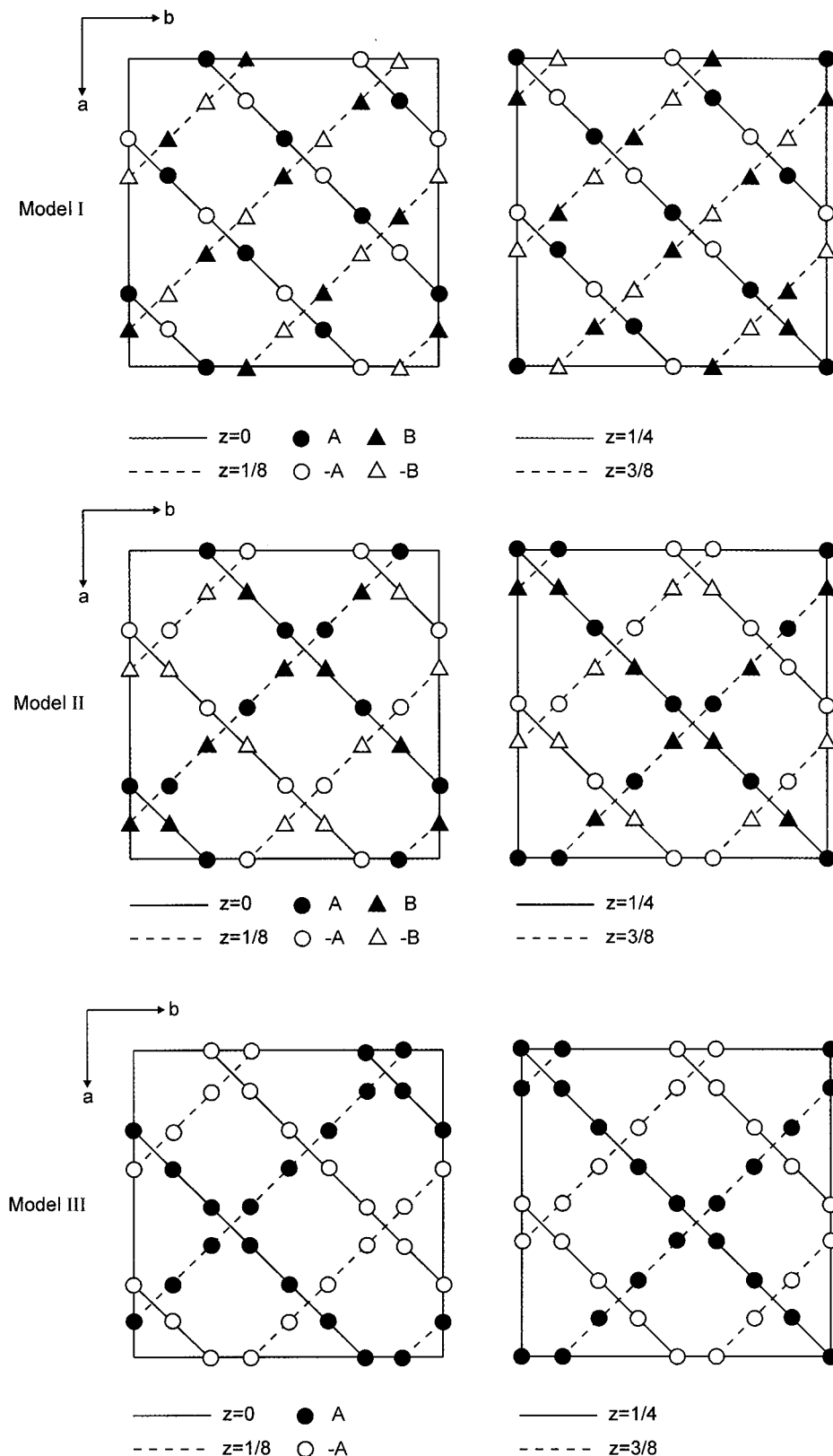


Figure 16. Three possible models for the spin structure in λ - MnO_2 , consistent with $k = (\frac{1}{2}\frac{1}{2}\frac{1}{2})$ shown in projection for half of the magnetic cell at planes $z = 0, 1/8, 1/4,$ and $3/8$. The moments in the second half of the cell are reversed. Circles and triangles correspond to different magnetic sublattices; black and white fills relate moments that are antiparallel. Models I and II have been proposed previously for GeNi_2O_4 ¹² and GeCo_2O_4 .¹³

β - MnO_2 is an interesting material in its own right although it appears that its characterization is somewhat incomplete. It is well established that a complex, antiferromagnetic spiral type magnetic order sets in below $T_N = 92$ K.^{15,16} This feature can be traced to the

Mn sublattice topology, body centered tetragonal, and that the first and second neighbor exchange constants

(15) Yoshinori, A. *J. Phys. Soc. Jpn.* **1959**, *14*, 807.

(16) Ohama, N.; Hamaguchi, Y. *J. Phys. Soc. Jpn.* **1971**, *30*, 1311.

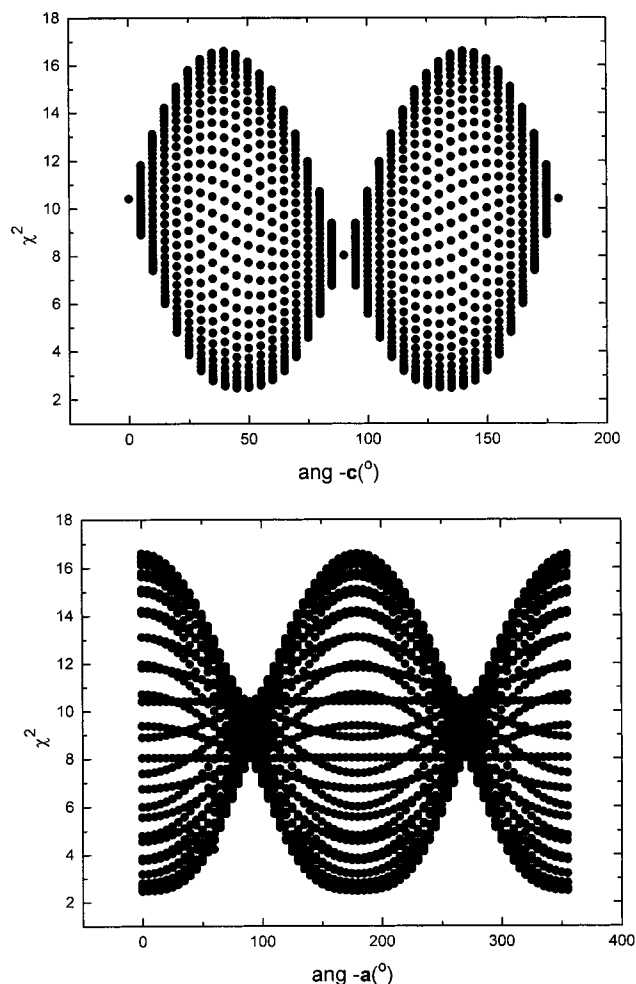


Figure 17. χ^2 values for the Model III refinement plotted against angles of the unit magnetic vector from the (lower) *a*-axis (ang-*a*), and from the (upper) *c*-axis (ang-*c*).

Table 2. Comparison of Exchange Pathways in β -MnO₂, λ -MnO₂, and Y₂Mn₂O₇

compound	neighbor	number	pathway	Mn-Mn distance, Å	angles, deg
β -MnO ₂	1st (J_1)	2	Mn-Mn	2.871	
		2	Mn-O-Mn	2.871	99
	2nd (J_2)	8	Mn-O-Mn	3.424	131
λ -MnO ₂	3rd (J_3)	4	several	4.396	
	1st (J_1)	6	Mn-Mn	2.84	
	6	Mn-O-Mn	2.84	96	
Y ₂ Mn ₂ O ₇	2nd (J_2)	6	Mn-O-O-Mn	4.923	94,134
	3rd (J_3)	6	several	5.684	
	1st (J_1)	6	Mn-Mn	3.505	
		6	Mn-O-Mn	3.505	132
	2nd (J_2)	6	Mn-O-O-Mn	6.065	144
3rd (J_3)	6	several	7.000		

are both negative and similar in magnitude, leading to a type of magnetic frustration between the body-centered spin and its eight neighbors. Good estimates of J_1/k (nearest neighbor) and J_2/k (next nearest neighbor) exchange constants are available from inelastic neutron scattering, -8.9 and -5.5 K, respectively. More distant pathways of which there are several of similar magnitude, can be collected as $J_3/k = +1.3$ K.¹⁶

Less well established are the parameters describing the paramagnetic regime with values of $\theta_c = -1050$ K and $C = 3.78$ mol/emu-K.¹⁶ It is unlikely that these can be correct because the maximum possible value for C for Mn⁴⁺, $S = 3/2$, is 1.87 emu-K/mol. This result indicates that θ_c is overestimated as well. Further support for such a view comes from a comparison of a calculated value for θ_c from the known exchange constants according to:

$$\theta_c/k = 2S(S+1)/3[2.5(2J_1 + 8J_2)] = -154 \text{ K}$$

The origin of this discrepancy has not been established, but it is likely that the true Curie-Weiss regime does

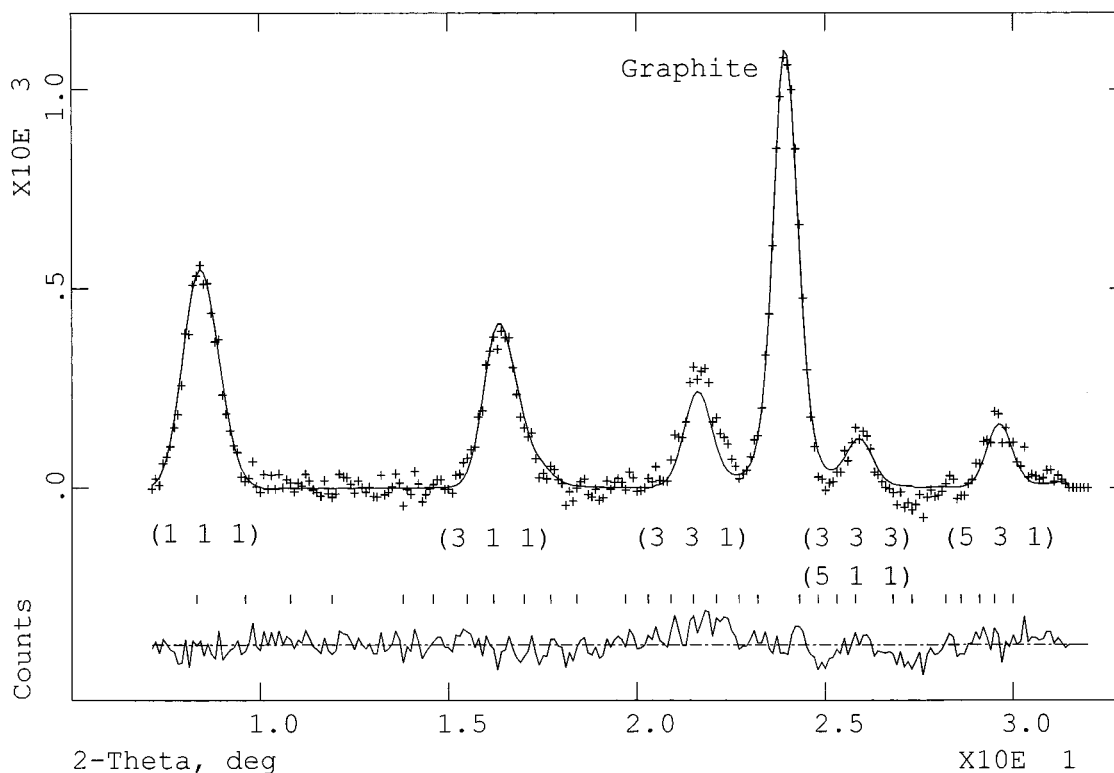


Figure 18. The experimental data and refined profile for λ -MnO₂, based on Model III ($\chi^2 = 1.57$ and $R_{wp} = 5.02\%$).

not obtain below 300 K, the maximum temperature of the measurements quoted in ref 16.

Upon examination of Table 2, it is clear that the nearest-neighbor exchange pathways are essentially identical for β -MnO₂ and λ -MnO₂, as expected given the common structural feature of octahedral edge-sharing. Sharp differences appear in the second-neighbor pathways, with the β -phase showing a much shorter Mn–Mn distance and a simpler Mn–O–Mn superexchange linkage than the λ -phase. In fact, even the third neighbors are closer in β -MnO₂ than the second neighbors in λ -MnO₂. This result suggests as a reasonable working hypothesis, the assumption that J_1 is the same in β - and λ -MnO₂ but that the J_2 and J_3 routes are relatively more important in the β -phase. On this basis, one can estimate an expected value for the Curie–Weiss θ in λ -MnO₂, neglecting J_2 , J_3 , etc., of -134 K, which is not far from the observed -104 K. That $J_1 < 0$ is a necessary condition for geometric frustration on the Mn corner-sharing tetrahedral lattice (often called the pyrochlore lattice). That $|\theta|/T_N$ is not large may result from the fact that the further neighbor interactions are positive or weakly negative. It is now very well known from many theoretical studies of the pyrochlore lattice that for the condition $J_1 < 0$ and $J_n = 0$, $n > 1$, no long-range order (LRO) can exist.^{5,6} LRO appears as a result of including more distant neighbor interactions.⁶

Y₂Mn₂O₇, the other relevant material to be compared here, is even more unusual. It shows spin glasslike behavior below ~ 17 K with no LRO.¹¹ The Curie–Weiss constants are also remarkable ($\theta_c = 41$ K), indicating that the exchange interactions sum to a ferromagnetic value. In Y₂Mn₂O₇, one has the same Mn⁴⁺ ion on the same pyrochlore lattice but with very different oxygen positions and connectivity for the octahedra; that is, edge sharing for λ -MnO₂ but corner sharing for Y₂Mn₂O₇. As a result, all of the Mn–Mn neighbor distances are significantly longer than in λ -MnO₂. Note from Table 2 that the J_2 pathway for β -MnO₂ and the J_1 pathway for Y₂Mn₂O₇ are very similar, implying that J_1 should be negative for the latter, which is again a necessary condition for geometric frustration and is consistent with the observed spin glass behavior. A negative J_1 is also in accord with a previous analysis of the diffuse magnetic neutron scattering in Y₂Mn₂O₇ which also indicated that the J_n , $n > 1$, were positive or ferromagnetic, thus rendering plausible the observed,

positive θ_c .¹¹ That λ -MnO₂ orders whereas Y₂Mn₂O₇ does not, may be traceable to the much longer Mn–Mn distances in the latter but a qualitative understanding is not presently available.

Finally, it is also worth noting that the properties of both λ -MnO₂ and Y₂Mn₂O₇ illustrate that the ratio criterion $|\theta_c|/T_{N,g} \gg 1$ for the assessment of magnetic frustration is far from a necessary condition. In neither case is this ratio greater than 3, whereas the importance of geometric frustration is clearly demonstrated for both. This result is especially true for Y₂Mn₂O₇, which shows no LRO while $|\theta_c|/T_g = 2.4$.

Summary and Conclusions

λ -MnO₂, a metastable form of manganese dioxide, better formulated as Li_xMnO₂ with $x < 0.1$, is characterized magnetically for the first time. It is shown to order antiferromagnetically with $T_N = 30$ – 32 K, depending slightly on preparation conditions. Evidence for the importance of geometric frustration, as might be expected from the Mn sublattice topology, is found from three observations. First, the nearest neighbor exchange, J_1 , is negative, as deduced from the similarity of the superexchange pathways with those in β -MnO₂. An antiferromagnetic J_1 is a necessary condition for geometric frustration on a tetrahedral lattice. Second, the short-range ordered thermal regime is unusually broad as seen in deviations from the Curie–Weiss law below $T > 4T_N$ and in the persistence of incommensurate diffuse magnetic scattering up to $T = 2T_N$. Finally, the magnetic structure below T_N is very complex with 128 spins per magnetic unit cell. That λ -MnO₂ shows LRO whereas the pyrochlore Y₂Mn₂O₇ does not may be traced to the much expanded Mn sublattice in the latter, which diminishes the relative importance of interactions beyond the nearest neighbor range.

Acknowledgment. The work at McMaster was supported by the Natural Sciences and Engineering Research Council of Canada. We also thank McMaster University for direct support of the McMaster Nuclear Reactor, and Dr. Zin Tun for assistance with the neutron scattering experiments in a magnetic field at the Chalk River Nuclear laboratories.

CM9801789